ELSEVIER

Chemical Engineering and Processing 41 (2002) 445–462

Chemical Engineering and Processing

www.elsevier.com/locate/cep

Hardware selection and design aspects for reactive distillation columns. A case study on synthesis of TAME

R. Baur, R. Krishna *

Department of Chemical Engineering, University of Amsterdam, Nieuwe Achtergracht 166, 1018 WV Amsterdam, The Netherlands

Received 15 May 2001; received in revised form 21 June 2001; accepted 2 August 2001

Abstract

We have carried out a step-by-step design study of a reactive distillation (RD) column for synthesis of tertiary-amyl ether (TAME) in order to investigate the influence of the choice of hardware on column design. Two different types of internals are compared: active Raschig rings and catalytic bales. Firstly, an equilibrium (EQ) stage model is used to obtain conceptual column design parameters. Detailed mass transfer and pressure drop calculations are then carried out to determine the column diameter and heights of the reactive and non-reactive sections of the RD column. Active Raschig rings have superior mass transfer characteristics but poorer pressure drop characteristics as compared to catalytic bales and therefore yield shorter and fatter column configurations. The detailed hardware configuration is finally checked with a rigorous nonequilibrium (NEQ) stage model to ensure that the designs are adequate and to investigate scope for further improvement. Our study underlines the importance of using NEQ models for column design and optimization. EQ stage models provide only initial estimates of column designs. The chosen column configurations must be carefully checked with rigorous NEQ models. Furthermore, our study reveals that the amount of catalyst used in the reactive section needs to be carefully chosen; excess of catalyst could lead to promotion of the reverse reaction of TAME to the reactants.

Keywords: Reactive distillation; Equilibrium stage model; Nonequilibrium stage model; Multiple steady states; Tert-amyl ether synthesis; Column hardware; Hydrodynamics; Mass transfer; Flooding

1. Introduction

Reactive distillation (RD) is an old idea that has received renewed attention in recent years; witness the recent reviews of Doherty and Malone [1,2] and Taylor and Krishna [3]. In the area of RD column design, research has mainly been focussed on aspects such as conceptual design with the aid of residue curve maps [1,2,4], steady-state multiplicity and bifurcations [5–8], development of equilibrium (EQ) stage and rigorous nonequilibrium (NEQ) steady-state and dynamic models [9–27]. Only more recently has attention been paid to hardware design aspects and the hydrodynamics and mass transfer in tray and packed columns [28–40].

For heterogeneously catalysed RD processes, hardware design poses many challenges [3]. The catalyst particle sizes used in such operations are usually in the 1–3 mm range. Larger particle sizes lead to intra-particle diffusion limitations. To overcome the limitations of flooding during counter-current vapour–liquid contacting, the catalyst particles have to be enveloped within wire gauze structures. Two commonly used structures in industry are:

1. Catalyst particles sandwiched between corrugated sheets of wire gauze [29–34]. Such structures are being licensed by Sulzer, called KATAPAK-S, and Koch-Glitsch, called KATAMAX. They consist of two pieces of rectangular crimped wire gauze sealed around the edge, thereby forming a pocket of the order of 1–5 cm wide between the two screens. These catalyst 'sandwiches' or 'wafers' are then bound together.
2. Catalyst particles enclosed in cloth wrapped in the form of bales [35–37].

The pressure drop and mass transfer characteristics of these two structures are similar [41] and the major

* Corresponding author. Tel.: +31-20-525-7007; fax: +31-20-525-5604.

E-mail address: krishna@its.chem.uva.nl (R. Krishna).

0255-2701/02/$ - see front matter
PII: S0255-2701(01)00166-0

difference between the above two structures is with respect to the radial dispersion characteristics. The KATAPAK and KATAMAX structures have very high radial dispersion coefficients [30,34] because of the criss-crossing construction.

Another alternative hardware choice for heterogeneous RD processes is to use standard packed column internals such as Raschig rings and makes these catalytically active; this is the strategy adopted by Flato and Hoffmann [42] and Sundmacher and Hoffmann [43]. Correlations for pressure drop and mass transfer for such packings are available in the literature [44–48].

The major objective of the present paper is to consider the various factors governing the choice of hardware for heterogeneously catalysed RD processes and to provide guidelines for making the proper choice. To illustrate the various considerations we undertake the specific design study of an RD column for synthesis of tertiary-amyl ether (TAME) using two specific hardware choices: catalytic bales and active Raschig rings. A further objective is to examine the need for rigorous NEQ models in RD column design.

2. Synthesis of TAME: reaction kinetics, thermodynamics and design specifications

TAME is formed by reversible, acid-catalysed, exothermic reaction of iso-amylenes (IA), consisting of the isomers 2-methyl-1-butene (2M1B) and 2-methyl-2-butene (2M2B), with methanol

$$\text{methanol} + 2\text{M1B} \leftrightarrow \text{TAME} \quad (1a)$$

$$\text{methanol} + 2\text{M2B} \leftrightarrow \text{TAME} \quad (1b)$$

The reaction kinetics has been studied by two different groups in Clausthal [4,49–51] and in Helsinki [52–54]. In our design study we use the forward reaction rate constants as presented by the Clausthal group; the reaction kinetics is described by a Langmuir–Hinshelwood rate expression in terms of the liquid phase activities [4,49–51]. The reaction equilibrium constant has been calculated according to Rihko and Krause [52]. In addition to the above two reactions, the two iso-amylenes undergo isomerization according to:

$$2\text{M1B} \leftrightarrow 2\text{M2B} \quad (2)$$

In our simulations we implemented the kinetics of isomerization as presented by Oost, Sundmacher, Hoffmann and others [4,49–51]. The catalyst activity has been specified by 900 eq$[H^+]$ m^{-3}; the overall catalyst volume depends on the type of packing and voidage in the column.

The process scheme used in our design study essentially follows that of Subawalla and Fair [36] and is shown in Fig. 1. The flow scheme consists of a pre-reactor followed by an RD column. The use of an isothermal pre-reactor is advantageous because high overall

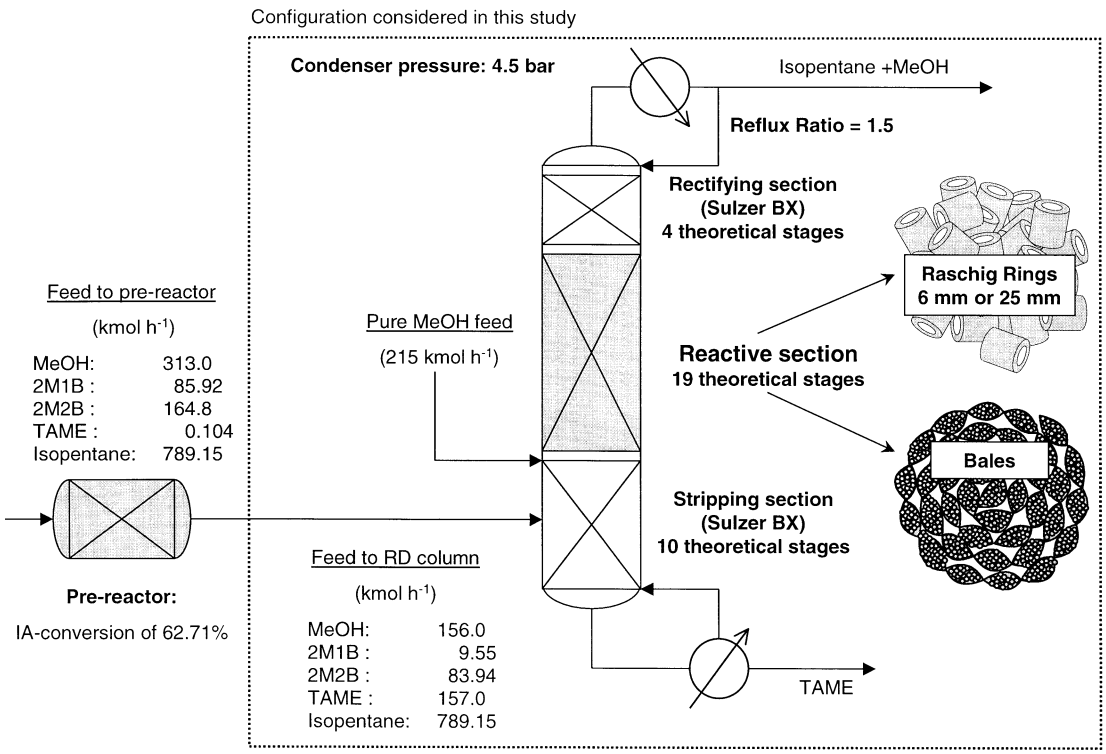

Fig. 1. Column configuration including a pre-reactor adapted from Subawalla and Fair [36].

Table 1
UNIQUAC binary interaction parameters adopted from Subawalla and Fair [36] and parameters for the extended Antoine equation based on the Aspen Plus data bank

UNIQUAC binary interaction parameters Component i	Component j	$b_{ij}/[K^{-1}]$	$b_{ji}/[K^{-1}]$
Methanol	2-methyl-1-butene	54.4	−788.85
Methanol	2-methyl-2-butene	28.82	−757.37
Methanol	TAME	75.15	−511.92
Methanol	Isopentane	−9.34	−670.42
2-methyl-1-butene	2-methyl-2-butene	−6.85	3.8
2-methyl-1-butene	TAME	−41.65	20.71
2-methyl-1-butene	Isopentane	82.98	−98.81
2-methyl-2-butene	TAME	−16.61	1.042
2-methyl-2-butene	Isopentane	63.71	−81.44
TAME	Isopentane	107.92	−144.72

Parameters for the extended Antoine equation. The parameters are taken from the Aspen plus data bank[a]

$$\ln(P_{sat}) = a + \frac{b}{T} + c\,\ln(T) + dT^{e}$$

Component	a	b	c	d	e
Methanol	82.718	−6904.5	−8.8622	7.47×10^{-6}	2
2-methyl-1-butene	97.33	−5631.8	−12.589	1.5395×10^{-2}	1
2-methyl-2-butene	83.927	−5640.5	−9.6453	1.11×10^{-5}	2
TAME	62.342	−5911.7	−5.8464	1.61×10^{-17}	6
Isopentane	72.35	−5010.9	−7.883	$8.98\times\times10^{-6}$	2

[a] Remark: P_{sat} is given in Pa and T in K.

TAME production rates can be obtained when the IA conversion in the pre-reactor is in the range 55–65%. In our study we assume a pre-reactor with an IA conversion of 62.7%, identical to that assumed by Subawalla and Fair [36]. Subawalla and Fair [36] considered a feed stream to the pre-reactor to consist of four inert components: isopentane, *n*-pentane, 1-pentene and 2-pentene. In order to reduce the complexity of the system we decided to consider only a single inert component, isopentane. Although the boiling points of the inert components differ, by about 8 K at 4.5 bar pressure, the choice of a single inert component does not significantly alter the thermodynamic behaviour. The activity coefficients for the inert C_5 components are close to unity and show almost ideal behaviour. The binary mixture of methanol and isopentane reveals a single minimum-boiling azeotrope ($x_{MeOH} = 0.269$ at $P = 4.5$ bar), just as found between methanol and the four C_5 inert components used in the Subawalla–Fair study. The UNIQUAC model with the binary parameters presented in Subawalla and Fair [36] are used to describe the thermodynamic non-ideality of the mixture. The vapour pressure is calculated by the extended Antoine equation. Table 1 lists the parameters used for simulation and design.

The process design specifications have been summarized in Table 2. Essentially we aim for a minimum IA conversion of 94%, maximum TAME impurity in top product of 50 ppm and a minimum TAME purity of 99.6% in the bottoms product from the RD column. Subawalla and Fair [36] determined the conceptual design parameters, such as number of theoretical stages in each section, reflux ratio and catalyst load by successive iterations using an EQ stage model until the pro-

Table 2
Process specifications and the conceptual column design used for designing the hardware of the column

Design specifications		
Minimum desired IA conversion	94	%
Maximum top TAME impurity	50	ppm
Minimum TAME purity in product	99.6	% mol mol^{-1}
Percent of flooding	80	%
Conceptual column design		
Number of theoretical stages:		
In the rectifying section	4	
In the reactive zone	19	
In the stripping section	10	
Reflux ratio	1.5	
Reboiler load	17.6	MW
Operating pressure	4.5	bar
Feed location:		
Pure MeOH feed located on stage	24	
Pre to reacted feed located on stage	29	
Catalyst specifications:		
Catalyst activity	900	eq$[H^+]$ m^{-3}
Catalyst volume	36	m^3
IA conversion	96.79	%
TAME impurity in the distillate	5.36	ppm
TAME purity in the product flow rate	99.9	% mol mol^{-1}

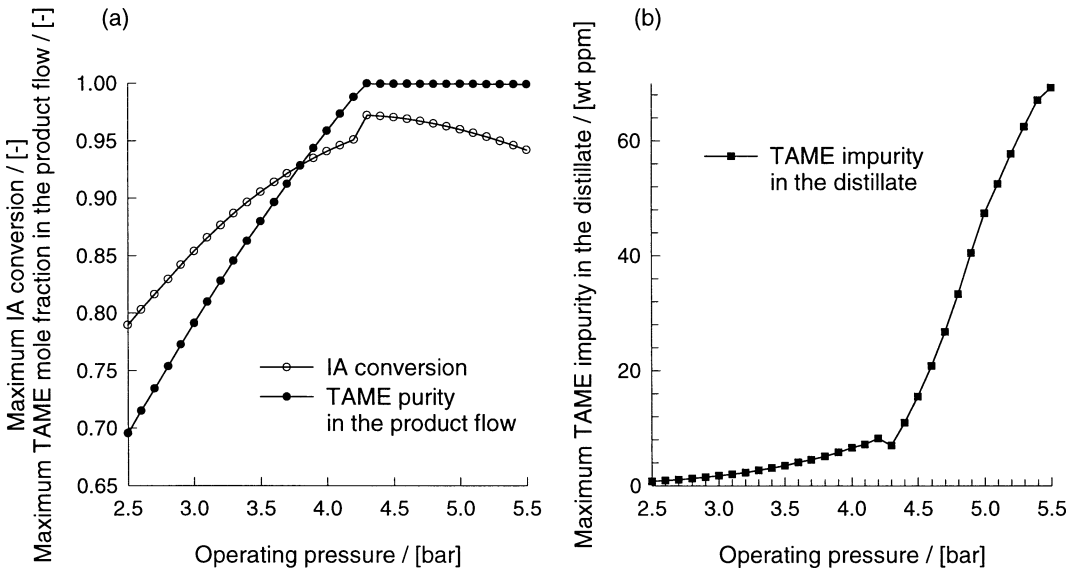

Fig. 2. Maximum values for (a) IA conversion, TAME purity in the product flow and (b) TAME impurity in the distillate for reboiler loads within a range of 17 and 19 MW. Note the values are local maximum belonging to different reboiler loads.

cess specifications are satisfied. Initial estimates for these calculations, like the number of stages and reflux ratio, are obtained from Fenske–Underwood short-cut calculations [2,44]. These considerations lead to a choice of four equilibrium stages in rectifying section, 19 reactive stages (each of which is in thermodynamic equilibrium) and ten equilibrium stages in the stripping section. The reflux ratio is chosen to be 1.5. The methanol feed was placed below the reactive section of the RD column, whereas the premixed feed, from the pre-reactor, which contains 157 kmol h^{-1} of TAME, is located in the middle of the stripping section. One should ensure that TAME in the pre-reacted feed is stripped off before it reaches the reactive section, otherwise it will revert back to IA and methanol at the bottom of the reactive section. Table 2 summarizes the conceptual column design, which will be used for the hardware design, and the process specifications.

With these specifications we proceed with a step-by-step column design procedure with the two different internals chosen; this step-by-step procedure is essentially the one suggested by Subawalla and Fair [36]. In the first step we use the EQ stage model to study the influence of operating pressure and reboiler load on column specifications.

3. Step 1: Use of EQ stage model to fix column pressure and reboiler load

The choice of the operating pressure is a trade-off between conversion and separation requirements. Increasing pressure causes increased reaction rates and a shift of chemical equilibrium due to higher boiling point temperatures in the reactive zone. On the other, increasing column pressure reduces the relative volatility. Increased pressure results in larger MeOH feed requirements whereas lower pressure requires higher demand of catalyst load in order to meet the desired specifications. Keeping both the catalyst load and MeOH feed flow constant we investigated the influence of the operating pressure on conversion and separation requirements. Using the EQ stage model (described extensively in the literature [9–27]) along with the column specifications in Table 2, we varied the operating pressure and investigated its influence on the TAME conversion and TAME mole fraction in the bottom product; the results are shown in Fig. 2(a). The active catalyst volume was taken to be 36 m^3. The plots in Fig. 2 show the local maxima when the reboiler load ranges from 17 to 19 MW at constant operating pressure. In Fig. 2(b) we note that the TAME impurity in the top product of the RD column increases sharply when the operating pressure increases beyond 4.5 bar. Low operating pressures result in lower boiling point temperatures in the reactive section and lower maximal attainable TAME purity in the bottoms flow rate. On the other hand, high operating pressure, say above 5 bar, will also significantly increase the TAME impurity in the distillate due to lower relative volatility and higher methanol requirements for the azeotropic mixture. Therefore, operating the column at a pressure between 4.3 and 5 bar provides a potential setup that might satisfy all process specification. Furthermore, it is worth mentioning that our EQ model simulations show that the RD column exhibits multiple steady states at operating pressures above 4.2 bar for the reboiler loads under consideration. It is beyond the scope of this

paper to discuss steady state multiplicity. Interested readers are referred to the paper by Mohl et al. [25].

On the basis of the results shown in Fig. 2, we choose an operating pressure of 4.5 bar. The process design specifications are all met when operating at a reboiler load of 17.6 MW; see Table 2. For 4.5 bar pressure and 17.6 MW reboiler load, Fig. 3(a) shows the corresponding liquid mole fraction profiles along the column height. Fig. 3(b) shows the TAME production rate along the reactive section. In the rectifying section the MeOH–isopentane azeotropic composition is nearly reached with 4 theoretical stages. The 19 theoretical stages in the reactive section appears to be sufficient to achieve a high IA-conversion (96.78%) and remove TAME in order to avoid TAME decomposition. The stripping section consists out of ten theoretical stage and provides a good recovery of 2M2B. Furthermore, ten theoretical stages appear to be necessary to bring the TAME purity in the bottom product to 99.9%.

Using the EQ model we also studied the bifurcation behaviour using the reboiler load as a continuation parameter. The results are shown in Fig. 4 as a plot of TAME purity versus IA conversion. This plot is helpful to see how the product specifications are met. The gray shaded area denotes the region for which process specifications in Table 2 are fulfilled. As can be seen from the figure increasing reboiler load results in higher TAME product purity in the bottoms product flow rate. Reasons for this are increased internal flow rates which facilitates the separation between isopentane and TAME in the stripping section. On the other hand higher reboiler loads also cause undesired lower bottom product flow rates as well as a possible drop in conversion. To illustrate this we also included the TAME production rates per catalyst volume along the reactive section for three steady states; see the insets to Fig. 4. The production rates exhibit typical profiles. At a reboiler load of 17.55 MW the production rates increase monotonically from the center of the reactive section towards its end, close to the stripping section. Increasing the reboiler load to 17.6 MW results in a maximum TAME production close to the bottom of the reactive section. Further increase of the reboiler load to 17.8 MW even causes TAME decomposition at the very end of the reactive section. For a reboiler load of 18 MW, the design specifications are no longer met and we note a sharp drop in IA conversion. This is triggered by a complex mechanism. It is observed that the isopentane mole fractions along the column height decrease for increasing reboiler loads. This also implies that methanol and TAME concentration are increased in the lower part of the reactive section. High TAME concentrations inhibit TAME production and even might result in TAME decomposition, as it is observed for reboiler load of 17.8 MW. Further, bearing in mind that the reaction order of methanol is negative, an excess of methanol in the reactive section is possibly slowing down the forward reaction rates. As can be

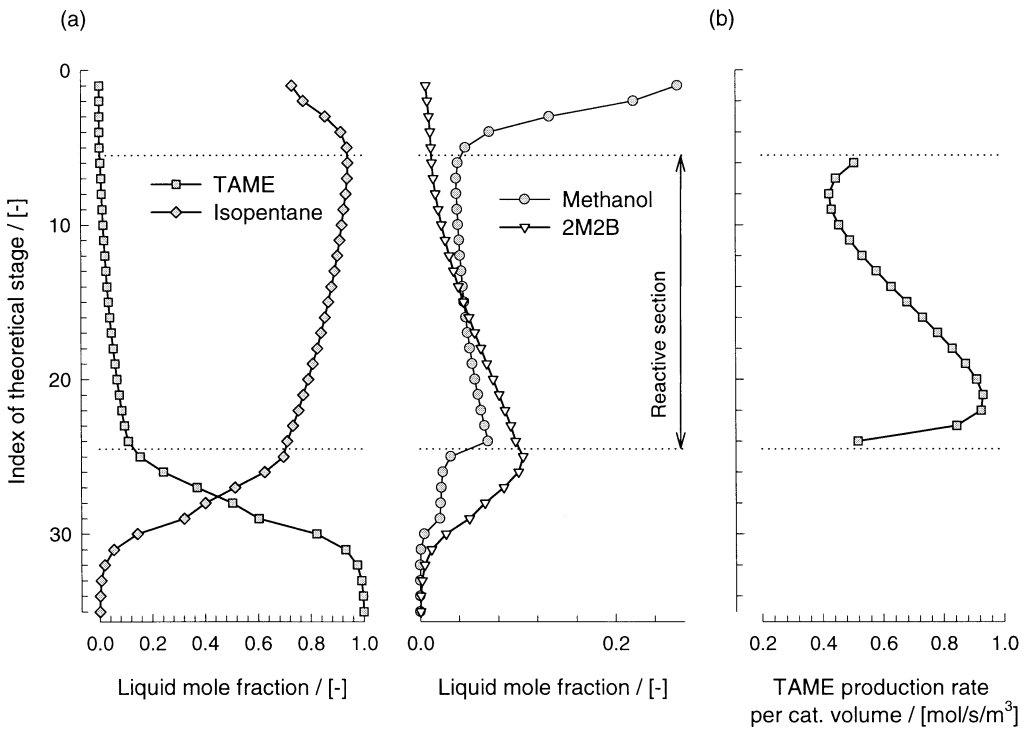

Fig. 3. Steady state profiles of EQ-model simulations: (a) composition profiles and (b) TAME productions rate. The reboiler load is set at 17.6 MW.

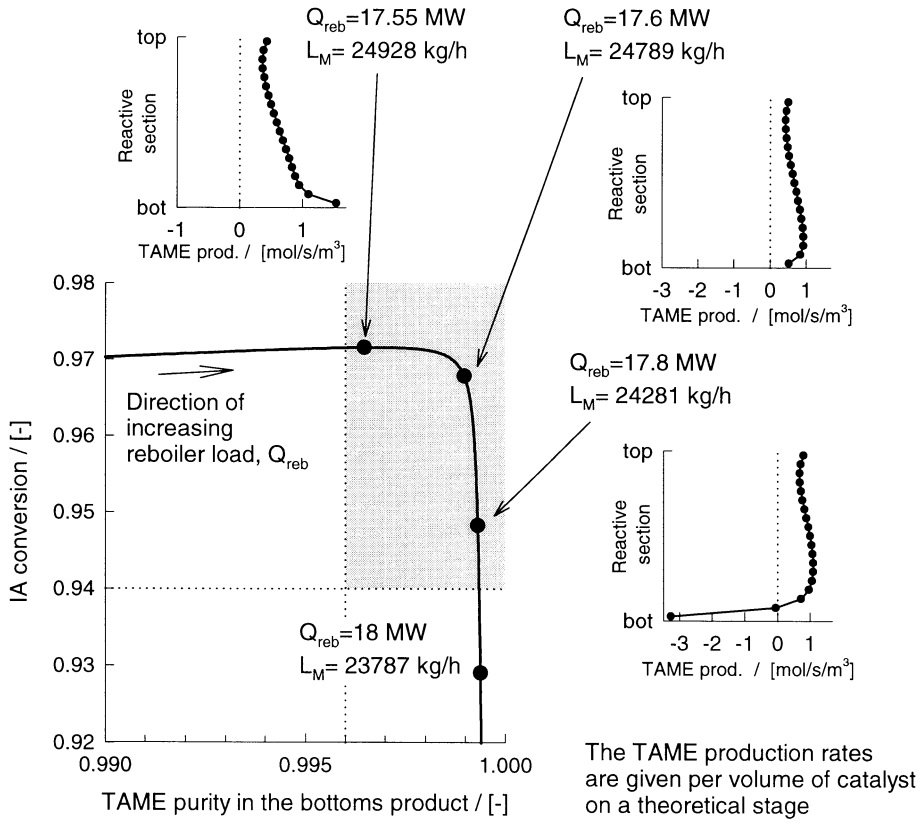

Fig. 4. Bifurcation diagram in the IA-conversion and TAME bottoms product purity sub-space when the reboiler load, Q_{reb}, is varied. The symbols denote steady states at reboiler load and product mass flow rate specified. The gray area denotes the region for which the specifications are satisfied.

seen in Fig. 3, the methanol concentration increases slightly towards the bottom of the reactive section, since the methanol feed is located below the reactive section. Hence, the core TAME production shifts towards the rectifying section where the main TAME formation takes place when the reboiler load is increased. In the bottom section less reactants are consumed. In the event of TAME decomposition, reactants may actually be formed at the bottom of the reactive section. This mechanism in turn causes a higher internal recycle of reactants and, therefore, lowers isopentane composition. This is also indicated when considering the overall conservation of mass. The bottoms product flow rates are decreasing with increasing reboiler duty and so the distillate mass flow has to increase. Considering that methanol and isopentane mole fractions in the condenser are close to their azeotropic compositon and that almost all isopentane is recovered in the distillate, the increase in distillate mass flow has to be realized by unreacted iso-amylenes.

The plot shown in Fig. 4 is important when we proceed further with the detailed design and choice of column internals.

4. Step 2: Determination of column diameter and height

For the reactive section we consider two choices: catalytic bales and active Raschig rings. For the calculation of the column diameter and height with catalytic bales we use the correlations presented by Subawalla et al. [35]. For calculating the mass transfer within the catalytic bales, Subawalla et al. [35] consider three mechanisms for mass transfer: (1) mass transfer within the packing; (2) mass transfer due to wall effects; and (3) mass transfer to drops in the open channels. A detailed study of the three mass transfer contributions shows that the mass transfer within the packings is the controlling contribution. Therefore we neglect mass transfer from drops and due to wall effects. The catalyst particles within the bales are not fully wetted and we use the Bornhütter and Mersmann correlation [55] to determine the wetted packing area. In case of the catalytic active Raschig Rings we consider two cases, rings with a nominal size of 1/4 and 1 in. Pressure drop and mass transfer are calculated using the correlations presented by Billet and Schultes [47,48].

For the non-reactive rectifying and stripping sections we choose the highly efficient Sulzer BX packing. The design correlations for Sulzer BX packing are taken from the literature [56,57]. A summary of the correlations used and the key parameters are listed in Table 3.

The column diameter depends predominantly on the pressure drop, on the maximum percentage of flooding and the liquid and vapour loads. The maximum percentage of flooding was specified to be 80%. An estimate for the maximum liquid and vapour load in each section is obtained from simulation of EQ model for the conceptual design (with reboiler load of 17.6 MW). These loads are listed together with other physical properties in Table 4. Table 5 presents the correlations that have been used to calculate physical properties; further details are available in Kooijman and Taylor [58] and on the ChemSep website: www.chemsep.org. In general, pressure drop correlations are expressed in terms of liquid and vapour superficial velocities and, therefore, the pressure drop depends implicitly on the

Table 3
Correlations and specification used for the packings

	Raschig rings 1/4 in.	Raschig rings 1 in.
Specifications and correlations used for Raschig rings		
Void fraction (–)	0.64	0.68
Packing area ($m^2\ m^{-3}$)	600	190
Pressure drop correlation	Billet and Schultes [48]	
Mass transfer model	Billet and Schultes [47]	
Specifications and correlations used for Bales		
Void fraction (–)	0.76	
Packing area ($m^2\ m^{-3}$)	169	
Pressure drop correlation	Subawalla et al. [36]	
Mass transfer model liquid holdup	The computation of the irrigated and dry pressure drop is based on the data given in Subawalla et al. [36]. Mass transfer due to drops and wall effects are neglected. Hence only mass transfer in the packing is considered. The correlation of Bornhütter and Mersmann [55] is used to compute the wetted packing area.	
Specifications and correlations used for Sulzer BX		
Void fraction (–)	0.9	
Packing area ($m^2\ m^{-3}$)	492	
Channel flow angle (°)	60	
Channel side (mm)	8.9	
Pressure drop correlation	Bravo et al. [56]	
Mass transfer model	Rocha et al. [57]	

Table 4
Properties and correlations used to estimate column diameter and HETP

Description	Rectifying section	Reactive section	Stripping section
Max liquid load ($m^3\ s^{-1}$)	0.0607	0.0613	0.1245
Max vapour load ($m^3\ s^{-1}$)	4481	4540	4771
Internal vapour flow rate (kmol s^{-1})	0.75–0.78	0.73–0.76	0.62–0.73
Internal liquid flow rate (kmol s^{-1})	0.46–0.49	0.41–0.49	0.4–0.77
Vapour density (kg m^{-3})	10.9–11.6	11.3–11.7	11.8–15
Liquid density (kg m^{-3})	571–604	569–593	588–633
Key component 1	MeOH	Isopentane	Isopentane
Key component 2	Isopentane	TAME	TAME
Vap. diffusivity $\mathcal{D}^V$ ($m^2\ s^{-1}$)	2.1×10^{-6}	1×10^{-7}	1.30×10^{-6}
Liq. diffusivity $\mathcal{D}^L$ ($m^2\ s^{-1}$)	1.33×10^{-8}	8.1×10^{-9}	1.2×10^{-8}
Slope of equilibrium line (m)	0.07–1.9	0.26–0.29	0.3–3.1

The estimates are based on EQ to model simulation at a reboiler load at 17.6 MW.

Table 5
Correlations for calculating physical properties

Description	Correlation
Vapour component density	Soave–Redlich–Kwong EOS
Liquid component density	Hankinson–Thomson
Vapour component viscosity	DIPPR
Liquid component viscosity	Letsou–Stiel
Vapour diffusion coefficients	Fuller–Schettler–Giddings
Surface tension	DIPPR
Maxwell–Stefan model	Described in Taylor and Krishna [45]

A detailed description of the listed methods can be found in Kooijman and Taylor [58].

cross-sectional area, i.e. on the column diameter (squared). Using the liquid and vapour loads obtained from the conceptual design we can iteratively obtain a minimum column diameter for which the constraint of maximum 80% flooding is fulfilled. This procedure is applied to correlations of each type of packing in the reactive section and to the correlations for Sulzer BX packing in the non-reactive sections. The results are summarized in Table 6 and presented in Fig. 5. Fig. 5 shows the pressure drop curves against the F-factor for the optimized column diameter. The large filled circles denote the maximum allowed F-factor for each packing type (from considerations of 80% of flooding). As can be expected from comparison of the packing voidages, the Raschig ring with a nominal size of 1/4 in. requires the largest column diameter of 6 m. The column diameter is significantly reduced to 4.5 m when 1 in. Raschig rings are used. Further reduction of the diameter to 3.3 m is obtained with catalytic bales. Furthermore, when designing the column one should keep in mind that the Raschig rings predict a much steeper increase of the pressure drop with the F-factor than catalytic bales; see

Table 6
Estimated column diameter and section heights for Raschig rings and Bales

	Rectifying section (m)	Reactive section (m)		Stripping section (m)
Column diameter				
Raschig rings 1/4 in.	–	6		–
Raschig rings 1 in.	–	4.5		–
Bales	–	3.3		–
Sulzer BX	2.8	–		3.2
Section height		From HETP	From catalyst volume	
Raschig rings 1/4 in.	–	3.9	3.5	–
Raschig rings 1 in.	–	4.3	7.1	–
Bales	–	17.8	17.4	–
Sulzer BX	1.0		–	2.2

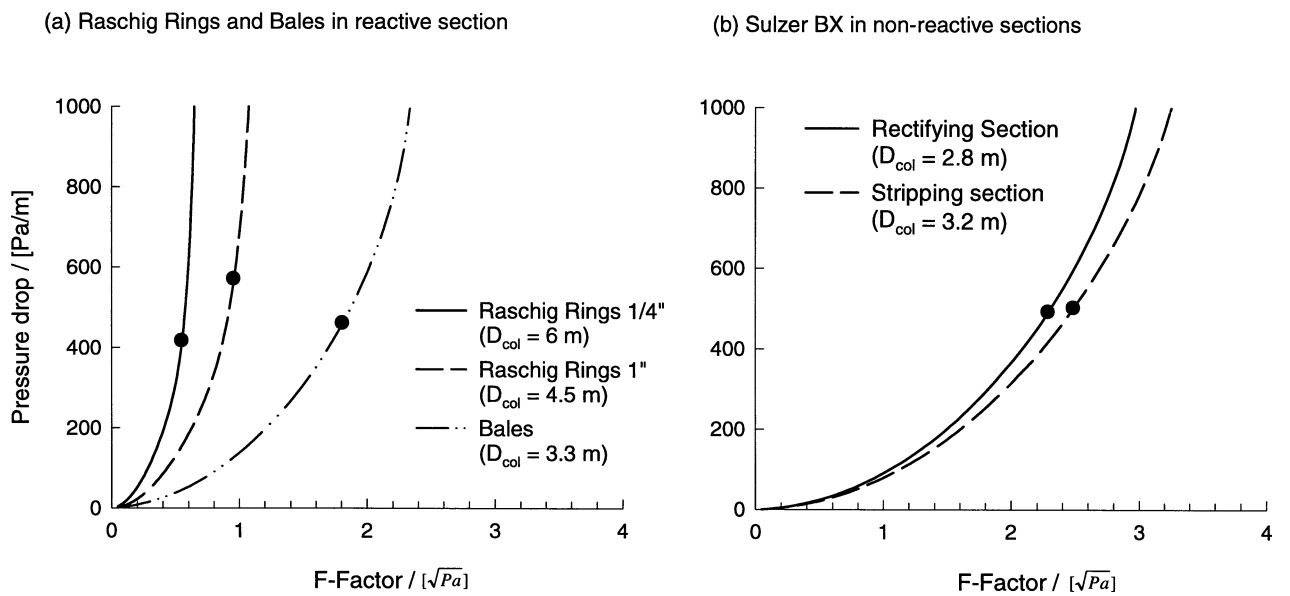

Fig. 5. Pressure drop versus F-Factor at constant maximum liquid load. The reboiler load is set at 17.6 MW. The filled black circles denote the design at 80% flooding and maximum vapour load. The maximum liquid and vapour loads per section are listed in Table 4.

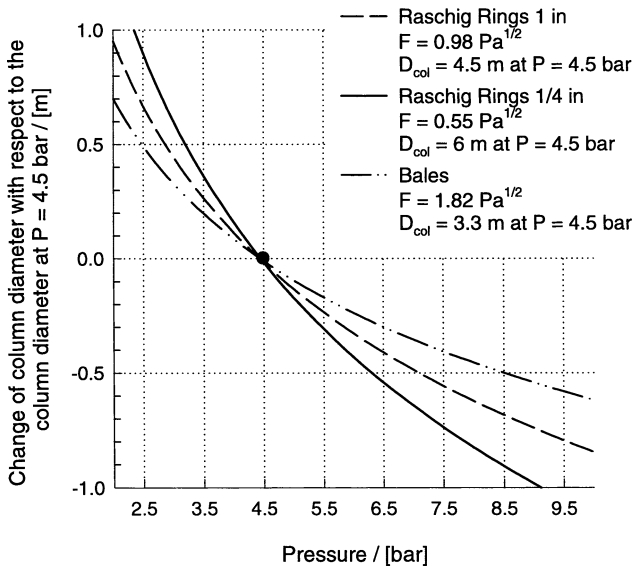

Fig. 6. Influence of the pressure on the estimated column diameter when the design F-factor and the maximum molar load is assumed to be constant for varying pressure. The molar vapour load is assumed to be 792 mol s^{-1} and the vapour density was computed for a representative concentration in the reactive section at dew point temperature ($y_{MeOH} = 0.145$, $y_{IA} = 0.048$, $y_{TAME} = 0.01$, $y_{isopentane} = 0.797$).

Fig. 5(a). Hence, Raschig Rings with a nominal size of 1/4 in. are most sensitive to possible flooding when the design F-factor (vapour load and density) for instance is exceeded due to disturbances or a change in the operation point, a consideration that should be taken into account when designing control systems for the column.

Comparing the values for the column diameter obtained in the reactive section with the ones from non-reactive sections using the Sulzer BX packing ($D_{col} = 2.8$ m for rectifying section and $D_{col} = 3.0$ m for stripping section) shows that the bottleneck for choosing the column diameter is in all cases the flooding in the *reactive* section. Flooding of the Sulzer BX packing in the non-reactive section cannot be expected for the chosen design loads; see Fig. 5(b). Furthermore, when the choice is made for Raschig rings in the reactive section then the expensive Sulzer BX packing in the non-reactive sections will be operated well below flooding. There is clearly a mismatch in the choice of active Raschig rings in the reactive section with use of Sulzer BX packing in the non-reactive sections. One could contemplate using cheaper random packings in the non-reactive sections in this case; this option was however not worked out in detail in the present study. Swaging of the column, i.e. using different column diameters in different sections, is not a viable option because of the high costs especially for operation at elevated pressures.

The operating pressure was fixed in the foregoing section based on thermodynamic and reaction kinetic considerations. The choice of the operating pressure also affects the hardware design due to change in the vapour density. Higher pressure will result in higher density what reduces the column diameter. In order to illustrate this we estimated the change of the design column diameter with regard to the base case. Fig. 6 shows this change in column diameter when the pressure is varied and the design F-factor (corresponds to 80% flooding at $P = 4.5$ bar) and molar flow rate are kept constant. Increasing or decreasing pressure (as long as the reaction kinetics and thermodynamic considerations do not restrict this) is a trade off between operational and investment costs. On one hand, reducing pressure will decrease the operational costs but also will decrease investments due lower construction costs. On the other hand the investment costs will increase because the column diameter increases also.

The next step is to determine the heights of the three separate sections in the RD column. For this purpose we need to estimate the height equivalent of theoretical plate (HETP) for the various chosen packings. In order to estimate HETP we chose for each section two key components. In the rectifying section the key components are MeOH and isopentane. For the reactive section and the stripping section we chose the inert isopentane and the product TAME. The HETP for the binary key components has been calculated form the binary mass transfer coefficient as described in standard textbooks; e.g. Stichlmair and Fair [44]. The transfer coefficients for catalytic bales were obtained from Subawalla and Fair [36]. The physical properties are taken from the EQ-model simulations of the conceptual design (see Table 3); the diffusivity values are specificed in Table 4. In order to illustrate the difference in mass transfer behaviour between Raschig rings and bales, we plotted the number of theoretical stages per meter versus the F-factor at a liquid load of 0.050 m^3 s^{-1}. Raschig Rings with a nominal size of 1/4 in. are much more efficient than 1 in. Raschig rings or bales. For both 1/4 and 1 in. Raschig rings, increase in the superficial vapour velocity causes an increase in the vapour mass transfer coefficients, which control the overall mass transfer. The number of theoretical plates per meter packing for Raschig rings increases sharply beyond the flooding point. The situation with respect to catalytic bales is quite different; here the liquid phase resistance is quite important. With increasing superficial vapour velocity, i.e. F-factor, the stripping factor (mV l^{-1}) increases. This causes a significant reduction in the contact time between the vapour and the liquid contained inside the bales. The liquid phase mass transfer coefficient is significantly reduced. This reduction compensates for the increase in the vapour phase mass transfer coefficient with increasing vapour load. The

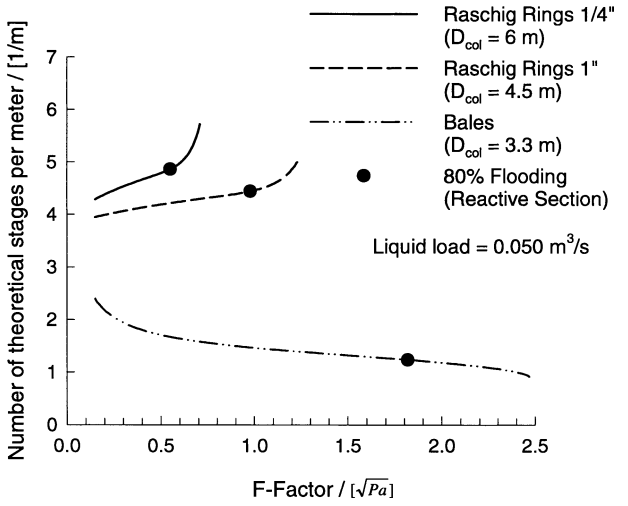

Fig. 7. Number of theoretical stages per meter vs. F-factor. The liquid load is kept constant at a value of 0.05 $m^3\ s^{-1}$.

number of theoretical plates per meter packing is therefore almost independent of the F-factor for catalytic bales.

Fig. 7 emphasises the superior mass transfer characteristics of Raschig rings compared to bales; this contrasts with the much poorer pressure drop characteristics witnessed in Fig. 5.

Qualitatively the situation can be understood as follows. The vapour–liquid contacting with Raschig rings is very intense as the vapour is in direct contact with the falling liquid films (and drops). This leads to intense momentum exchange and high pressure drop. But the interphase mass transfer with Raschig rings is excellent. With catalytic bales, the situation is totally different. The catalyst particles are located within rolled-up cloth layers and the liquid flowing over the catalyst particles is not in direct contact with the vapour that flows through the open regions between the cloth layers. The vapour only comes into contact with the liquid at the cloth surface and some entrained liquid drops within the open channels. Consequently the pressure drop is low, but the vapour–liquid mass transfer is also low. Low pressure drop is not compatible with good mass transfer.

In the next step the heights of reactive and non-reactive sections are estimated applying the same HETP estimation procedure on each stage. The physical properties, such as molar flow rates, densities have been taken from the simulation of the conceptual design; see Fig. 8. It is noticeable that the HETP predictions for the non-reactive sections vary in all cases within a quite large range (0.1 up to 0.4 m). This spread is not observed for the reactive section where the variance of the HETP prediction is comparably small. The reason for this is the fact that stripping factors (the ratio of the slopes of the equilibrium line to that of the operating line, mV l^{-1}) is nearly constant in the reactive section but this is not the case in the non-reactive sections. Summarizing, the HETPs in each section gives indication of the section height. It turns out that the height of the Sulzer BX packing in the stripping and rectifying section are almost the same for each case. We find that the four theoretical stages in the rectifying section correspond to a height of about 1 m, whereas the ten theoretical stages in the stripping section correspond to a height of about 2.2 m. As expected the heights in the reactive section will differ depending on the chosen packing type. Using 1/4 in. Raschig Rings results in a section height of about 3.9 m and Raschig Rings with a nominal size of 1-in. demands a reactive section height of 4.3 m. The difference in height is much more evident when focussing on the bales packing. In order to match the 19 theoretical stages of the conceptual design a section height of 17.8 m is predicted in our calculations. A summary of the height requirements for the different sections is given in Table 6.

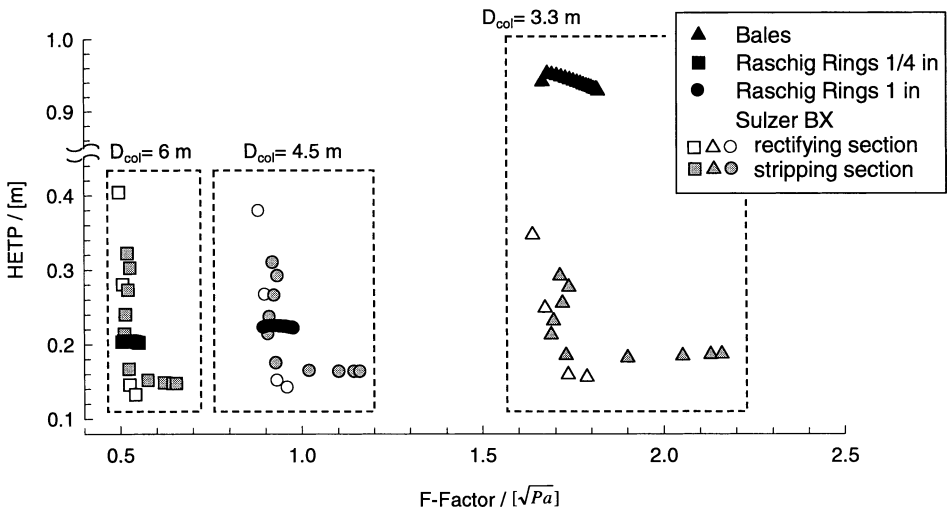

Fig. 8. HETP estimates as a function of the F-factor. The vapour and liquid loads are as specified in Table 4.

Table 7
Column configurations used for NEQ simulations

Description	Case 1	Case 2	Case 3	Case 4	Case 5
Column diameter (m)	6	4.5	3.3	3.3	3.3
Section height					
Rectifying section (m)	1	1	1	1	1
Reactive section (m)	3.9	7.1	17.8	12.8	12.8
Stripping section (m)	2.2	2.2	2.2	2.2	4.5
Total height (m)	7.1	10.3	21.0	16.0	18.3
Catalyst load (m^3)	36	36	36	26.275	26.275
Catalyst efficiency (eq m^{-3})	900	900	900	900	900
Packing type[a]					
Non-reactive sections	SBX	SBX	SBX	SBX	SBX
Reactive section	RR 1/4 in.	RR 1 in.	Bales	Bales	Bales
Reflux ratio	1.5	1.5	1.5	1.5	1.5
Reboiler load (MW)	17.74	17.65	17.88	17.88	17.88

[a] Remark: SBX, Sulzer BX; RR, Raschig rings.

The height of the reactive section is also determined by another constraint: the catalyst load required from activity considerations. We specified the catalyst load as the catalytic active volume, i.e. the overall ring or particle volume of the catalyst. For a given catalytic active volume, V_{cat}, the minimum section height, h, can be obtained from the volumetric constraint

$$h = 4\frac{V_{cat}}{(1-\varepsilon)\pi D_{col}^2} \quad (3)$$

where ε denotes the packing voidage. In the development of the conceptual design we have chosen 36 m^3 catalytic active packing volume. Using this volume determines the height requirements listed in Table 7. For the bales packing and the 1/4 in. Raschig Rings the minimum height do not exceed the estimations from the HETP calculations. This, however, is not true for Raschig Rings with a nominal size of 1 in. Hence in order to maintain the overall activity of the catalyst it is required to consider a more than 60% taller section than expected from the HETP estimations. Put another way the catalyst volume requirement is of overriding consideration in the determination of the reactive section height for the 1 in. Raschig Rings. For catalytic bales, the catalytic load requirements almost coincides with that from HETP considerations. Table 6 summarises the height requirements for various internals choices.

Clearly, for each case the more stringent requirement has to be met; this determines the chosen height of each section. The final chosen configurations are summarized in the first three columns in Table 7. In order to give a visual impression we draw the configurations for 1/4 in. Raschig Rings, 1 in. Raschig Rings and Bales packing in Fig. 9. Using 1/4 in. Raschig Rings results in a fat but short column, while incorporating catalytic bales packing will lead to a slim and tall column. Although the columns are designed for the same yield and product purity, the differences in column configuration are significant. A further remark to be made is that while use of 1/4 in. Raschig rings is justified for small diameter laboratory columns in experimental investigations, for industrial use we would prefer to use larger diameter rings which yield lower pressure drop. Pressure drop and flooding are important issues for commercial operation. In general, we would prefer to build tall slim columns to short and fat ones because the primary column cost determinant for high pressure systems, excluding column internals cost, is the column diameter and not the column height.

5. Step 3: Check chosen hardware design using rigorous NEQ model

Our column designs have been arrived at by use of an EQ stage model, along with HETP calculations for the different sections. The 'final' designs need to be checked by use of rigorous NEQ stage simulations to see if indeed the specifications are met. We therefore set up NEQ simulations of the three cases listed in the first three columns of Table 7; the details of the NEQ model are available in our earlier publications [11–17]. Each of the three cases has the same overall catalyst activity and volume (36 m^3). For 1/4 in. Raschig rings and catalytic bales we need to use additional inert particles/rings in order to fill the reactive section (to meet the constraint of separation stages) without increasing the overall catalyst activity. In practice, one might consider increasing the catalyst load or decreasing the section height slightly. This, however, would require a check whether a modified conceptual design would still satisfy the specifications. Such an iterative procedure was proposed by Subawalla and Fair [36]. Using 1 in. Raschig

rings, the minimum reactive section height due to the catalyst volume constraint exceeds the estimates from the HETPs. In this case the number of theoretical stage corresponds to approximately 30 (instead of 19 proposed by the conceptual design).

For setting up the NEQ-model we incorporated the pressure drop and mass transfer correlations per section and per packing type. Physical properties, which have been used, are listed in Table 5. The column has been discretized in slices. High concentration and temperature gradients in the non-reactive section suggest applying a finer grid there. We used 40 slices in the rectifying section, 50 slices in the stripping section and 38 slices in the reactive section. It turned out that the increasing the discretization did not alter the results. A coarser grid size, however, results in significant deviations. A total condenser is employed at the top of the column and a partial reboiler at the bottom. The reflux ratio was kept constant at 1.5, as specified in the conceptual design.

Fig. 10(a) and (b) shows the bifurcation diagram for the three configurations, along with the base case EQ-model of the conceptual design. The qualitative behaviour of the NEQ-models resembles the conceptual design using the EQ. In all three cases the NEQ model simulations show that the desired specifications cannot be met if the reboiler load is maintained at the conceptual design level of 17.6 MW; in each case the reboiler load has to be increased. For 1/4 in. Raschig rings a value of 17.74 MW is required, For 1 in. Raschig rings the value is 17.65 MW and for catalytic bales the reboiler load needs to be increased to 17.88 MW. Below these specified values the TAME purity in the bottoms product stream drops sharply; see Fig. 10(b). The HETP computation made use of EQ-model simulation at a design reboiler load of 17.6 MW. None of the NEQ models can recover such high purity and conversion at a reboiler load of 17.6 MW. Therefore, the reboiler loads have to be adjusted. Fig. 10(a) presents IA conversion versus bottoms TAME purity diagram for the three configurations (with adjusted reboiler loads) obtained from NEQ simulations. The bales and 1/4 in. Raschig Rings have, according to the HETP estimations, the same number of theoretical stages in each section. Nevertheless, model predictions in the region of interest differ significantly. Surprisingly, the NEQ-model predictions for 1 in. Raschig rings appears to be closer to predictions for 1/4 in. Raschig rings than predictions for bales packing, despite the fact that the number of theoretical stages in the reactive section is 60% higher (according to the HETP estimations).

Fig. 11 shows the steady state composition profiles for the three case studies; in this figure the vertical distance has been normalized to exactly coincide for the three cases. When focussing on the composition profiles one can see that there is hardly any difference between the two Raschig ring configurations; see Fig. 11(a). The same applies to the temperature profiles. Slightly higher molar vapour flow rates can be observed for 1/4 in. Raschig Rings compared with 1 in. Raschig Rings; see Fig. 11(b). This results from the fact that a configuration with 1/4 in. Raschig Rings requires a higher reboiler heat duty (17.74 compared to 17.65 MW) to meet the design specifications.

Although these differences are hardly visible in the composition and temperature profiles the effect on the

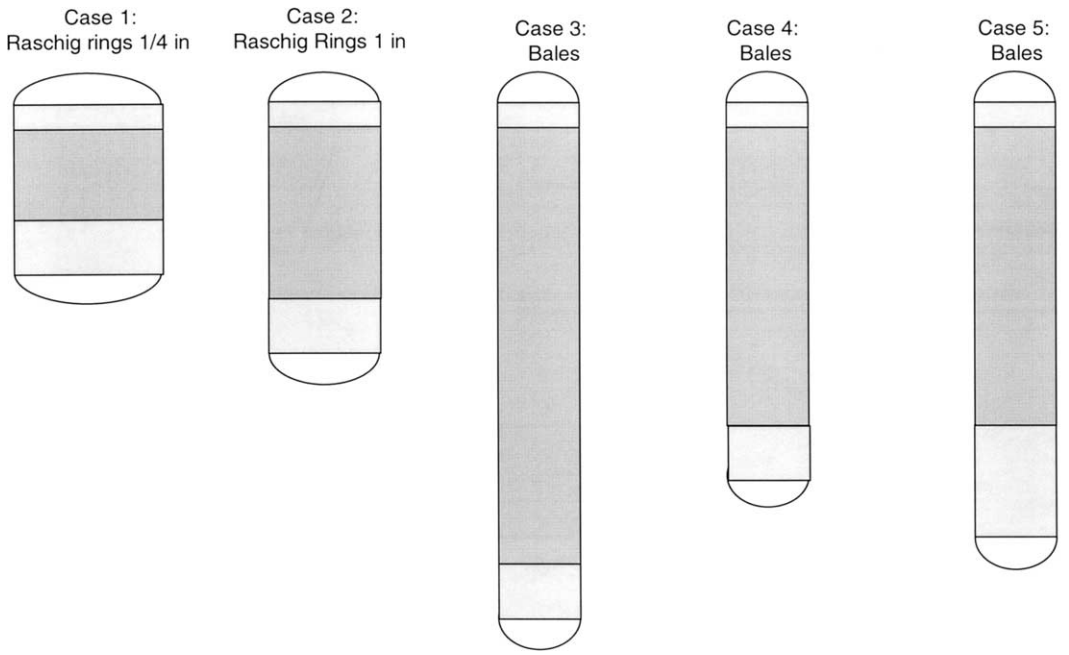

Fig. 9. Schematic of column configurations for the five cases shown in Table 7.

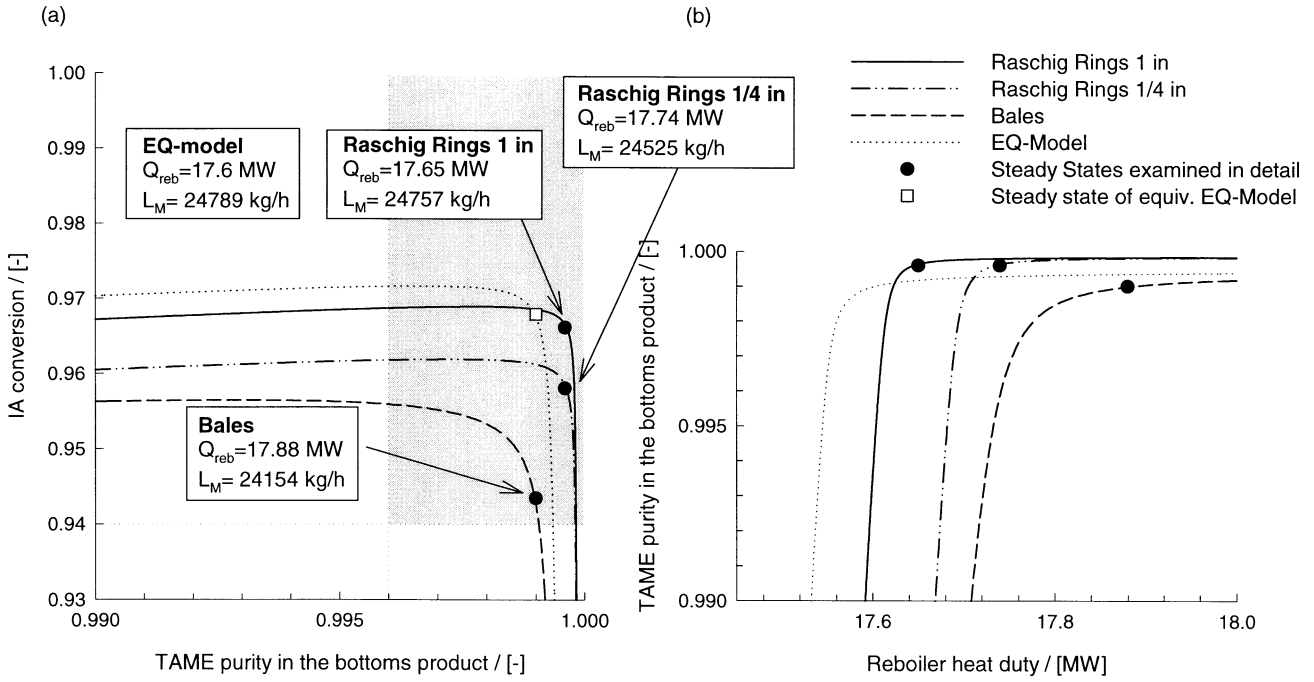

Fig. 10. Bifurcation diagrams for Cases 1, 2 and 3 in Table 7 obtained with varying reboiler loads. The results are presented in (a) IA conversion–TAME purity space and (b) TAME purity vs. reboiler load.

TAME production rates are more pronounced. As can be seen in Fig. 11(d) the extrema are more distinct in the case of 1 in. Raschig rings and so is the overall conversion higher. Fig. 12 shows the mass transfer rates of the reactants (a) methanol and (b) 2M2B along the reactive section in each of the 39 slices. The height of the reactive section with 1 in. Raschig rings exceeded with about 60% the height determined by the HETP estimations. This resulted in slightly higher mass transfer rates and production rates at a lower reboiler load than predicted for the 1/4 in. Raschig Rings.

Fig. 11(c) shows the pressure drop along the column height. The pressure drop computed in the reactive section for Raschig rings exceeds the one for bales. The non-reactive sections of the Raschig ring configurations are operating well below their flooding capacities. Furthermore, one should notice that the 1/4 in. Raschig Rings is operating very close to flooding. This is caused by the fact that the design load have been chosen for a reboiler load of 17.6 MW and not for reboiler load of 17.74 MW. Furthermore, 1/4 in. Raschig rings are much more susceptible to a rapid increase of pressure drop when the volumetric flow rates increase slightly; see also Fig. 5(a).

In case of bales packing we had to choose a reboiler load of 17.88 MW in order to meet the required specifications. The achieved conversion is lower than the conversion obtained for Raschig rings; see Fig. 10(a). This is caused due to TAME decomposition in the bottom part of the reactive zone; see Fig. 11(d). TAME decomposition in the bottom of the reactive section, observed in the bales configuration, is an undesired phenomena which indicates that the column configuration can be further optimized. The mechanism triggering TAME decomposition has been observed and described previously with EQ-model. Excess of methanol in the top of the reactive section favour the TAME production there, whereas increased mole fractions of the reactant in the bottom causes TAME to decompose. This is also indicated in Fig. 12 by the negative mass transfer rates for MeOH and 2M2B for the bales.

In order to optimize the configuration of bales packing we decreased the height of the reactive section and, therefore, the overall catalyst load until we obtained an evenly distributed TAME production rate in the reactive section at the same reboiler load. A reactive section height of 12.8 m results in an almost 30% lower catalyst load! The TAME production rates are shown as Case 4 in Fig. 13 and the detailed configuration is given in Table 7. The non-reactive sections have been kept the same as for Case 3. Evaluating the conversion and product purity for varying reboiler load, however, showed that the desired specifications have not been obtained; see Fig. 14. In a next step we increased the height of the stripping section in order to compensate the loss of separation due to the shortening of the reactive section. Increasing the height of the stripping section to 4.5 m meets the given specification as can be seen in the specification subspace in Fig. 14. Increasing the stripping section also does not affect the TAME production rates in the reactive section. As shown in

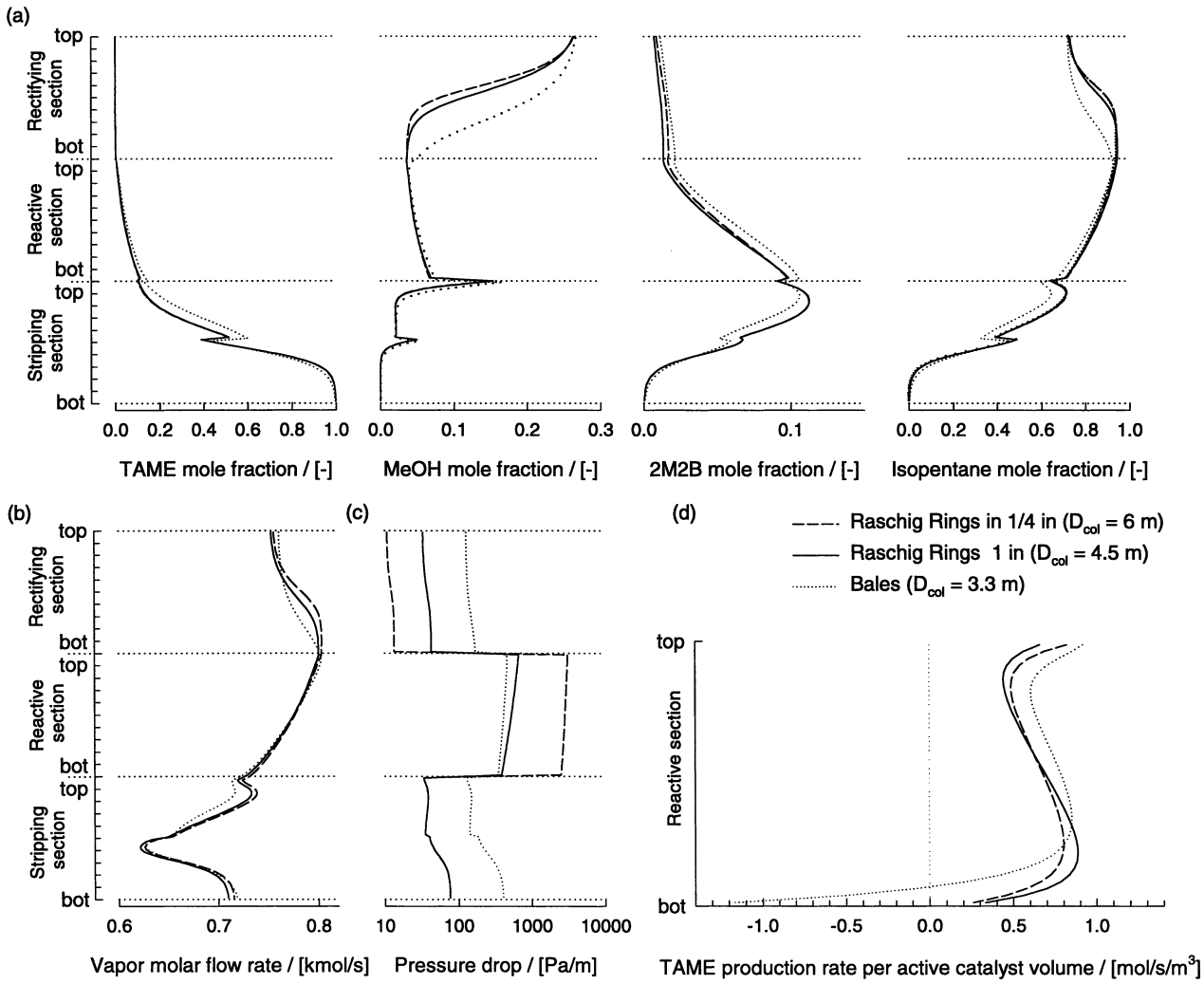

Fig. 11. Steady state profiles for the configuration case studies 1, 2 and 3 specified in Table 7. (a) Composition, (b) molar vapour flow rate, (c) pressure drop and (d) TAME production rate profiles for each case study.

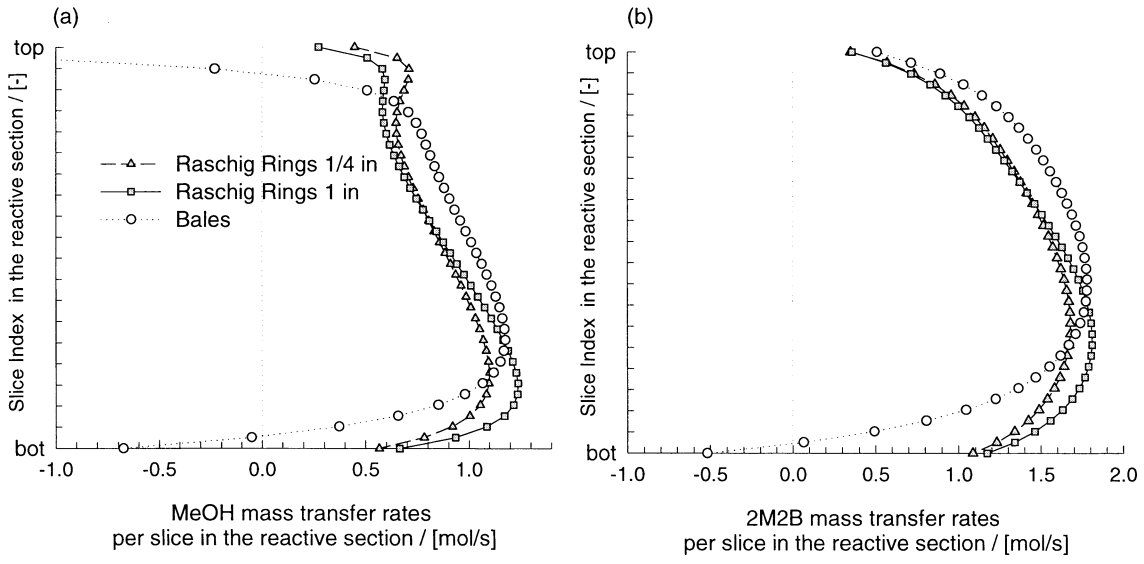

Fig. 12. Mass transfer rates of (a) methanol and (b) 2M2B in the reactive section. Comparison of Cases 1, 2 and 3.

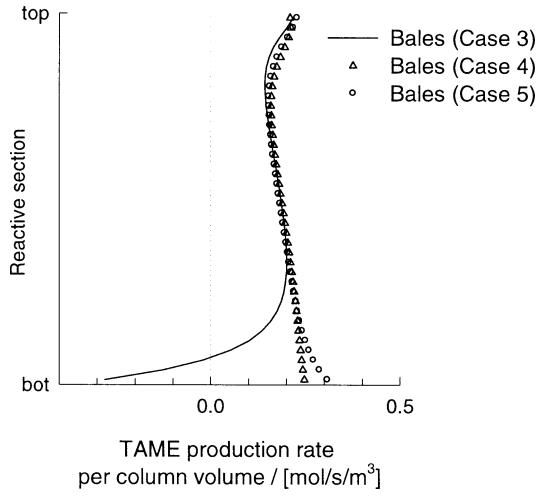

Fig. 13. TAME production rate in the reactive section for three column configurations, Cases 3, 4 and 5 containing bales; see Table 7. The reboiler load is fixed at 17.88 MW for all three cases.

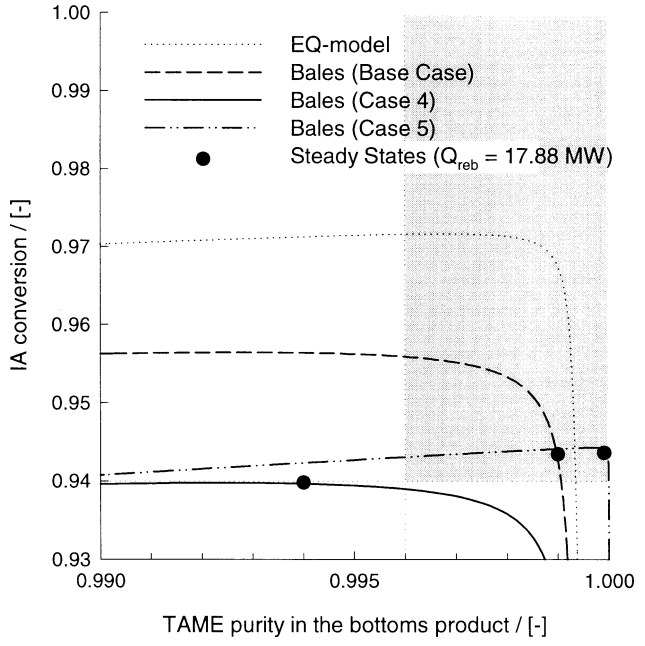

Fig. 14. Bifurcation diagram in the IA-conversion–TAME purity subspace for the three column configurations Cases 3, 4 and 5 containing bales in the reactive section; see Table 7.

Fig. 13 (Case 5) the TAME production rates slightly increases due to better removal of TAME in the bottom of the reactive section. The differences in various designs (Cases 3, 4 and 5) of column containing bales packing are substantial, as can be visualized in Fig. 9. Compared with the design obtained from the EQ-model, almost 30% of catalyst are saved and the overall column height is reduced by 2.7 m. Case 4 does not meet the specifications but Case 5 does.

The obvious advantages of the bales configuration with reduced catalyst load poses the question whether a modified conceptual design could have predicted such a column design. We modified the previous EQ-model by proportionally decreasing the reactive section (using a catalyst load of 26.735 m^3) and increasing the stripping section. Hence, the rectifying section contains 4, the reactive section 14 and the stripping section 20 theoretical stages. The pure methanol feed is located below the reactive section and the feed from the pre-reactor in the middle of the stripping section. Fig. 15 shows the predictions of the modified EQ-model in the specification subspace when the reboiler load is varied. The two markers in Fig. 15 denote the steady states for 17.88 MW. As noticed in the previous case for the conceptual design the high conversion predicted by the EQ-model and the NEQ-model for the modified bales configuration Case 5 are qualitatively similar but not quantitatively. For instance, the conversion at reboiler load of 17.88 MW seems to differ only slightly but focussing on the column profiles reveals larger differences. Fig. 16 shows the comparison between prediction of the EQ-model and the NEQ model for Case 5. The separation of TAME in the stripping section is much more pronounced for the EQ model that that predicted by the NEQ-model; see Fig. 16(a). This also affects the TAME production rates where the EQ-model predicts TAME decomposition in the lower part of the reactive section; see Fig. 16(b). However, a design with negative reaction rate would have been rejected. Hence, the design would focus on higher reboiler load in order to avoid TAME decomposition. In turn, the NEQ-model predicts rapidly dropping purity for such reboiler loads. This example shows that the valuable information obtained from conceptual design requires careful further studies with rigorous models reflecting column internals. The importance of using rigorous NEQ models is evident from Fig. 16.

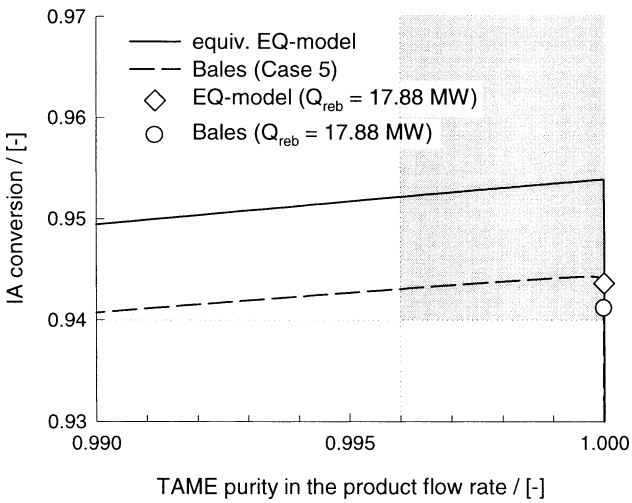

Fig. 15. Comparison between Case 5 in Table 5 and an equivalent EQ model ($N_{RSec} = 4$, $N_{ReSec} = 14$, $N_{StSec} = 21$) in the IA-conversion–TAME purity subspace. The catalyst load is $V_{cat} = 26.275$ m^3 for both cases.

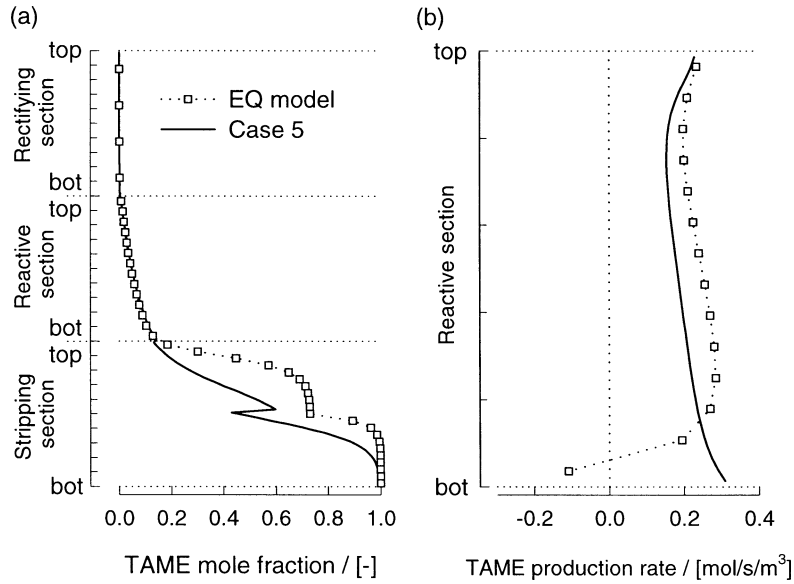

Fig. 16. TAME composition profile and TAME production rate along the dimensionless section heights for Case 5 in Table 5 and EQ-model ($N_{RSec} = 4$, $N_{ReSec} = 14$, $N_{StSec} = 21$).

6. Concluding remarks

We have carried out a step-by-step design study for synthesis of TAME in an RD column to investigate the influence of the choice of internals on column design. The following major conclusions can be drawn from this study.

1. Active Raschig rings have superior mass transfer characteristics but poorer pressure drop characteristics as compared to catalytic bales. This leads to shorter fatter column configurations; see Fig. 9. A detailed cost comparison needs to be made for the column configurations shown in Fig. 9 in order to arrive at the final choice. Such a cost comparison is not within the scope of our study.
2. EQ stage models provide only conceptual estimates of column designs. The chosen column configurations must be carefully checked with rigorous NEQ models. We have noted in particular that the reboiler load had to be increased beyond the conceptual estimate of 17.6 MW in order to obtain configurations meeting with the design specifications; see Fig. 10.
3. In the TAME case study we have demonstrated that conceptual design with bales (Case 3) can be improved substantially by reducing the catalyst load in the reactive section and increasing the separation capability of the stripping section; compare Cases 3 and 5 with bales in Table 7 and Fig. 13.
4. The limitations of the EQ model have been underlined in the simulation results given in Fig. 16 for Case 5. Both EQ and NEQ models predict nearly equal IA conversion and TAME purity. However, as can be seen in Fig. 16, the EQ model overestimates the separation capability in the stripping section and predicts TAME decomposition at the bottom of the reactive section.

Appendix A. Notation

D_{col}	column diameter (m)
$Đ_{i,j}$	Maxwell Stefan diffusivity ($m^2\ s^{-1}$)
h	height (m)
m	slope of the equilibrium line (dimensionless)
N	number of theoretical stages (dimensionless)
Q_{reb}	reboiler heat duty (W)
P	pressure (Pa)
U	superficial velocity ($m\ s^{-1}$)
V_{cat}	catalytic active volume (m^3)

Greek symbols

ε	voidage of the packing (dimensionless)

Subscripts

L	refers to the liquid phase
Rsec	rectifying section
ReSec	reactive section
StSec	stripping section
V	refers to the vapour phase

References

[1] M.F. Doherty, M.F. Malone, Reactive distillation, Ind. Eng. Chem. Res. 36 (2000) 4325–4334.

[2] M.F. Doherty, M.F. Malone, Conceptual Design of Distillation Systems, McGraw-Hill, New York, 2001.

[3] R. Taylor, R. Krishna, Modelling reactive distillation, Chem. Eng. Sci. 55 (2000) 5183–5229.

[4] C. Thiel, K. Sundmacher, U. Hoffmann, Residue curve maps for heterogeneously catalysed reactive distillation of fuel ethers MTBE and TAME, Chem. Eng. Sci. 52 (1997) 993–1005.

[5] R. Jacobs, R. Krishna, Multiple solutions in reactive distillation for methyl tert butyl ether synthesis, Ind. Eng Chem. Res. 32 (1993) 1706–1709.

[6] S.A. Nijhuis, F.P.M. Kerkhof, A.N.S. Mak, Multiple steady states during reactive distillation of methyl tert-butyl ether, Ind. Eng. Chem. Res. 32 (1993) 2767–2774.

[7] S. Hauan, T. Hertzberg, K.M. Lien, Multiplicity in reactive distillation of MTBE, Comput. Chem. Eng. 21 (1997) 1117–1124.

[8] T.E. Güttinger, M. Morari, Predicting multiple steady states in equilibrium reactive distillation. 1. Analysis of nonhybrid systems, Ind. Eng. Chem. Res. 38 (1999) 1633–1648.

[9] T.E. Güttinger, M. Morari, Predicting multiple steady states in equilibrium reactive distillation. 2. Analysis of hybrid systems, Ind. Eng. Chem. Res. 38 (1999) 1649–1665.

[10] E.Y. Kenig, A. Gorak, Modeling of reactive absorption using the Maxwell-Stefan equations, Ind. Eng. Chem. Res. 36 (1997) 4325–4334.

[11] R. Baur, A.P. Higler, R. Taylor, R. Krishna, Comparison of equilibrium stage and non-equilibrium stage models for reactive distillation, Chem. Eng. J. 76 (2000) 33–47.

[12] A. Higler, R. Taylor, R. Krishna, Modeling of a reactive separation process using a nonequilibrium stage model, Comput. Chem. Eng. 22 (1998) S111–S118.

[13] A.P. Higler, R. Taylor, R. Krishna, Nonequilibrium modelling of reactive distillation: multiple steady states in MTBE synthesis, Chem. Eng. Sci. 54 (1999) 1389–1395.

[14] A.P. Higler, R. Taylor, R. Krishna, The influence of mass transfer and liquid mixing on the performance of reactive distillation tray column, Chem. Eng. Sci. 54 (1999) 2873–2881.

[15] A. Higler, R. Krishna, R. Taylor, A non-equilibrium cell model for packed distillation columns. The influence of maldistribution, Ind. Eng. Chem. Res. 38 (1999) 3988–3999.

[16] A. Higler, R. Krishna, R. Taylor, Non-equilibrium cell model for multicomponent (reactive) separation processes, AIChE J. 45 (1999) 2357–2370.

[17] A. Higler, R. Krishna, R. Taylor, Non-equilibrium modelling of reactive distillation: a dusty fluid model for heterogeneously catalysed processes, Ind. Eng. Chem. Res. 39 (2000) 1596–1607.

[18] R. Baur, R. Taylor, R. Krishna, J.A. Copati, Influence of mass transfer in distillation of mixtures with a distillation boundary, Chem. Eng. Res. Des. Trans. I. Chem. E. 77 (1999) 561–565.

[19] R. Baur, R. Taylor, R. Krishna, Development of a dynamic nonequilibrium cell model for reactive distillation tray columns, Chem. Eng. Sci. 55 (2000) 6139–6154.

[20] R. Baur, R. Taylor, R. Krishna, Dynamic behaviour of reactive distillation tray columns described with a nonequilibrium cell model, Chem. Eng. Sci. 56 (2001) 1721–1729.

[21] R. Baur, R. Taylor, R. Krishna, Dynamic behaviour of reactive distillation columns described by a nonequilibrium stage model, Chem. Eng. Sci. 56 (2001) 2085–2102.

[22] R. Baur, R. Taylor, R. Krishna, Influence of column hardware on the performance of reactive distillation columns, Catal. Today 66 (2001) 225–232.

[23] K. Sundmacher, Reaktivdestillation mit katalytischen fuellkoerperpackungen-ein neuer Process zur Herstellung der Kraftstoffkomponente MTBE, Ph.D thesis, Universität Clausthal, 1995.

[24] L.U. Kreul, A. Gorak, P.I. Barton, Modeling of homogeneous reactive separation processes in packed columns, Chem. Eng. Sci. 54 (1999) 19–34.

[25] K.D. Mohl, A. Kienle, E.D. Gilles, P. Rapmund, K. Sundmacher, U. Hoffmann, Steady state multiplicities in reactive distillation columns for the production of fuel ethers MTBE and TAME: theoretical analysis and experimental verification, Chem. Eng. Sci. 54 (1999) 1029–1043.

[26] A. Kumar, P. Daoutidis, Modeling, analysis and control of ethylene glycol reactive distillation column, AIChE J. 45 (1999) 51–68.

[27] V.H. Agreda, L.R. Partin, W.H. Heise, High-purity methyl acetate via reactive distillation, Chem. Eng. Prog. No. 2 (1990) 40–46.

[28] A. Tuchlenski, A. Beckmann, D. Reusch, R. Düssel, U. Weidlich, R. Janowsky, Reactive distillation—industrial applications, process design and scale-up, Chem. Eng. Sci. 56 (2001) 387–394.

[29] J.L. DeGarmo, V.N. Parulekar, V. Pinjala, Consider reactive distillation, Chem. Eng. Prog. No. 3 (1992) 43–50.

[30] C. Van Gulijk, Using computational fluid dynamics to calculate transversal dispersion in a structured packed bed, Comput. Chem. Eng. 22 (1998) S767–S770.

[31] A.P. Higler, R. Krishna, J. Ellenberger, R. Taylor, Counter-current operation of a structured catalytically packed bed reactor: liquid phase mixing and mass transfer, Chem. Eng. Sci. 54 (1999) 5145–5152.

[32] J. Ellenberger, R. Krishna, Counter-current operation of structured catalytically packed distillation columns: pressure drop, holdup and mixing, Chem. Eng. Sci. 54 (1999) 1339–1345.

[33] P. Moritz, H. Hasse, Fluid dynamics in reactive distillation packing Katapak®-S, Chem. Eng. Sci. 54 (1999) 1367–1374.

[34] J.M. van Baten, J. Ellenberger, R. Krishna, Radial and axial dispersion of the liquid phase in a KATAPAK-S® structure: experiments vs CFD simulations, Chem. Eng. Sci. 56 (2001) 813–821.

[35] H. Subawalla, J.C. Gonzalez, A.F. Seibert, J.R. Fair, Capacity and efficiency of reactive distillation bale packing: modeling and experimental validation, Ind. Eng. Chem. Res. 36 (1997) 3821–3832.

[36] H. Subawalla, J.R. Fair, Design guidelines for solid-catalyzed reactive distillation systems, Ind. Eng. Chem. Res. 38 (1999) 3606–3709.

[37] M.M. Akbarnejad, A.A. Safekordi, S. Zarrinpashne, A study on the capacity of reactive distillation bale packings: experimental measurements, evaluation of the existing models, and preparation of a new model, Ind. Eng. Chem. Res. 39 (2000) 3051–3058.

[38] R. Krishna, J.M. Van Baten, J. Ellenberger, A.P. Higler, R. Taylor, CFD simulations of sieve tray hydrodynamics, Chem. Eng. Res. Des. Trans. I. Chem. E. 77 (1999) 639–646.

[39] J.M. Van Baten, R. Krishna, Modelling of sieve tray hydraulics using computational fluid dynamics, Chem. Eng. J. 77 (2000) 143–152.

[40] J.M. van Baten, J. Ellenberger, R. Krishna, Hydrodynamics of reactive distillation tray column with catalyst containing envelopes: Experiments vs. CFD simulations, Catal. Today 66 (2001) 233–240.

[41] P.J. Lebens, F. Kapteijn, S.T. Sie, J.A. Moulijn, Potentials of internally finned monoliths as a packing for multifunctional reactors, Chem. Eng. Sci. 54 (1999) 1359–1365.

[42] J. Flato, U. Hoffmann, Development and start-up of a fixed bed reaction column for manufacturing antiknock enhancer MTBE, Chem. Eng. Technol. 15 (1992) 193–201.

[43] K. Sundmacher, U. Hoffmann, Multicomponent mass transfer and energy transport on different length scales in a packed reactive distillation column for heterogeneously catalysed fuel ether production, Chem. Eng. Sci. 49 (1994) 4443–4464.
[44] J.G. Stichlmair, J.R. Fair, Distillation Principles and Practice, Wiley-VCH, New York, 1998.
[45] R. Taylor, R. Krishna, Multicomponent Mass Transfer, Wiley, New York, 1993.
[46] K. Onda, H. Takeuchi, Y. Okumoto, Mass transfer coefficients between gas and liquid phases in packed columns, J. Chem. Eng. Jpn. 1 (1968) 56–62.
[47] R. Billet, M. Schultes, Advantage in correlating packed column performance, Inst. Chem. Eng. Symp. Series No. 128, Volume 2, Institution of Chemical Engineers, UK, 1992, pp. B129–B136.
[48] R. Billet, M. Schultes, A physical model for the prediction of the liquid holdup in two phase countercurrent columns, Chem. Eng. Technol. 16 (1993) 370–375.
[49] C. Oost, K. Sundmacher, U. Hoffmann, The synthesis of tertiary amyl methyl ether (TAME): equilibrium of the multiple reactions, Chem. Eng. Technol. 18 (1995) 110–117.
[50] C. Oost, U. Hoffmann, The synthesis of tertiary amyl methyl ether (TAME): microkinetics of the reactions, Chem. Eng. Sci. 51 (1996) 329–340.
[51] K. Sundmacher, G. Uhde, U. Hoffmann, Multiple reactions in catalytic distillation processes for the production of the fuel oxygenates MTBE and TAME: analysis by rigorous model and experimental validation, Chem. Eng. Sci. 54 (1999) 2839–2847.
[52] L.K. Rihko, A.O.I. Krause, Kinetics of heterogeneously catalyzed tert-amyl methyl ether reactions in the liquid phase, Ind. Eng. Chem. Res. 34 (1995) 1172–1180.
[53] L.K. Rihko, P. Kiviranta Paakkonen, A.O.I. Krause, Kinetic model for the etherification of isoamylenes with methanol, Ind. Eng. Chem. Res. 36 (1997) 614–621.
[54] P. Kiviranta-Paakkonen, L. Struckmann, A.O.I. Krause, Comparison of the various kinetic models of TAME formation by simulation and parameter estimation, Chem. Eng. Technol. 21 (1998) 321–326.
[55] K. Bornhütter, A. Mersmann, Mass transfer in packed columns. The cylinder model, Chem. Eng. Technol. 16 (1993) 46–57.
[56] J.L. Bravo, J. Rocha, J.R. Fair, Distillation columns containing structured packings: a comprehensive model for their performance. 1. Hydraulic models, Ind. Eng. Chem. Res. 32 (1993) 641–651.
[57] J. Rocha, J.L. Bravo, J.R. Fair, Distillation columns containing structured packings: a comprehensive model for their performance. 1. Mass transfer model, Ind. Eng. Chem. Res. 35 (1996) 1660–1667.
[58] H.A. Kooijman, R. Taylor, The ChemSep book, Libri Books, 2001. See website: www.chemsep.org.